Dual contributions of analyte adsorption and electroosmotic inhomogeneity to separation efficiency in capillary electrophoresis of proteins

Laura Dhellemmes, Laurent Leclercq, Lisa Lichtenauer, Alisa Höchsmann, Michael Leitner, Andreas Ebner, Michel Martin, Christian Neusüß, Hervé Cottet

Dual contributions of analyte adsorption and electroosmotic inhomogeneity to separation efficiency in capillary electrophoresis of proteins

Laura Dhellemmes[1], Laurent Leclercq[1], Lisa Lichtenauer[2], Alisa Höchsmann[3], Michael Leitner[2], Andreas Ebner[2], Michel Martin[4], Christian Neusüß[3], Hervé Cottet[1*]

[1] IBMM, University of Montpellier, CNRS, ENSCM, Montpellier, France

[2] Institute of Biophysics, Johannes Kepler University Linz, Linz, Austria

[3] Faculty of Chemistry, Aalen University, Aalen, Germany

[4] PMMH, CNRS, ESPCI Paris-PSL, Sorbonne Université, Université de Paris, France

ABSTRACT: Improving separation efficiency in capillary electrophoresis (CE) requires systematic study of the influence of the electric field (or solute linear velocity) on plate height for a better understanding of the critical parameters controlling peak broadening. Even for poly(diallyldimethylammonium chloride) (PDADMAC)/poly(sodium styrene sulfonate) (PSS) successive multiple ionic-polymer layers (SMIL) coatings, which lead to efficient and reproducible separations of proteins, plate height increases with migration velocity, limiting the use of high electric fields in CE. Solute adsorption onto the capillary wall was generally considered as the main sources of peak dispersion explaining this plate height increase. However, experiments done with Taylor Dispersion Analysis and CE in the same conditions indicate that other phenomena may come into play. Protein adsorption with slow kinetics and few adsorption sites was established as a source of peak broadening for specific proteins. Surface charge inhomogeneity was also identified as a contribution to plate height due to local electroosmotic fluctuations. A model was proposed and applied to partial PDADMAC/poly(ethylene oxide) capillary coatings as well as PDADMAC/PSS SMIL coatings. Atomic force microscopy with topography and recognition imaging enabled the characterization of the PDADMAC/PSS SMIL surface.

Introduction

Capillary electrophoresis (CE) is a powerful analytical technique that separates and analyzes charged compounds based on their electrophoretic mobility in an electric field. As for any other separation technique, it is interesting to maximize separation efficiency to get the best of CE separations. This is crucial, especially for protein analysis for which the identification and quantification of protein variants require high plate numbers that can theoretically reach up to a million plates. Investigating and understanding the sources of peak broadening in CE calls for a systematic study of the influence of the electric field (or analyte linear velocity u) on plate heights H (1). This leads to typical H *vs* u plots, as observed in chromatography. The ascending part of the curve is generally interpreted as the presence of analyte adsorption onto the capillary surface, particularly for high molar mass compounds such as proteins (2-4). This can strongly limit separation efficiency, especially at high electric fields. It is therefore important to lower the H *vs* u slope p by reducing the sources of this dispersion.

Different ways of limiting the adsorption of analytes onto the capillary wall have been developed, including capillary coatings, which can be permanent, semi-permanent or dynamic (5). Among these, semi-permanent coatings are obtained from physically adsorbed polymers or double-chains surfactants (6-11) onto the capillary wall. In particular, successive multiple ionic-polymer layers (SMIL) are made up of several layers of polyelectrolytes which alternate between polycations and polyanions, and have been shown to be stable over a wide range of pH, as well as performant in terms of repeatability and separation efficiency (12).

In addition to adsorption, other possible sources of dispersion in CE include the presence of a radial temperature gradient (13), electromigration dispersion (14), capillary

coiling (15), and sample polydispersity (16). Variations in the electroosmotic flow (EOF) may also be contributing factors, since any defect in the flow profile leads to reduced separation efficiency (17,18).

Some authors cite the length of the electric double layer (EDL) as a reason the EOF can contribute to plate height (19,20). Indeed, the EDL, which is composed of free ions attracted by the immobile surface charge and a layer of mobile charges within the Debye length (typically 1-10 nm in CE), is thought to be negligible when compared to the channel radius (10-100 µm), generating a very thin sheath where the otherwise uniform plug-flow rapidly decreases. The Debye length varies with the ionic strength of the background electrolyte (BGE) (19), and may generate more dispersion in the case of very low ionic strength leading to double layer overlap for nanometer channels. But these cases remain very rare and do not apply in our current study (50 µm I. D. capillaries and a 2 M AcOH BGE of 6 mM ionic strength, corresponding to 4 nm Debye length). Several authors have tried to model this electroosmotic contribution to dispersion, with Griffiths and Nilson suggesting an empirical function (20), which was then generalized by Zholkovskij et al. (21):

$$H = \frac{2D\eta}{\varepsilon\zeta E} + \frac{2\varepsilon\zeta E}{\eta\kappa^2 D} g(\zeta) K \qquad (1)$$

where H is the plate height, D the analyte molecular diffusion coefficient, ε the BGE dielectric permittivity, κ the Debye parameter or inverse of the Debye length, η the BGE viscosity, ζ the electrical or zeta potential, and K a dimensionless geometrical factor which is equal to 0.5 for circular capillaries. Using the approximation $\frac{\varepsilon\zeta}{\eta} = \mu_{eo}$ for the electroosmotic mobility, and the typical values of D = 5×10^{-11} m²/s, μ_{eo} = -45 TU (Tiselius Unit, 1 TU = 10^{-9} m²V^{-1}s^{-1}), κ^{-1} = 4 nm, $g(\zeta)$ = 1 and E = 5×10^{4} V/m used in our experiments, the first term was found equal to 4×10^{-8} m, and the second 1×10^{-15} m. Therefore, only the first term of Eq. 1, which corresponds to axial diffusion, is relevant to our study.

Other authors have illustrated the impact of surface charge inhomogeneity on electroosmotic flow, with Ajdari concluding that convective hydrodynamic rolls are induced (22), and Long et al. stressing the long-range disturbance caused by a localized defect (23). Herr et al. brought to light the effect of surface inhomogeneity by studying the variations in EOF in coupled capillary sections with different ζ-potentials through the use of EOF-suppressing polymers, establishing experimental flow profiles with fluorescent dye (24). Similarly, it was demonstrated that adsorbed species on the capillary wall generated non-uniform zeta potential, disrupting both transport velocity and peak width (25).

In this work, sources of peak dispersion during protein separation by CE using SMIL coatings were investigated. The previously established model based on equilibrium adsorption (1) was applied and called into question in light of new results. Other possible causes of peak broadening such as electroosmotic fluctuations stemming from coating inhomogeneity were considered. A new model was proposed and tested using intentionally inhomogeneous partial capillary coatings, then generalized to SMIL coatings. For some proteins, increased plate height with increasing electric fields could be explained by adsorption with slow desorption kinetics. Finally, SMIL coatings were characterized by topography and recognition imaging (TREC)-atomic force microscopy (AFM), backing the model with experimental data about charge distribution and topography.

Theoretical part

A relationship giving the plate height in CE when there is a discontinuity in electroosmotic mobility in the capillary has been established. The full demonstration can be found in the Supporting Information (see SI Theoretical Part). It is important to note that only axial inhomogeneity was considered here, and assumed to be regularly distributed along the capillary surface, which is no doubt a simplified view of reality.

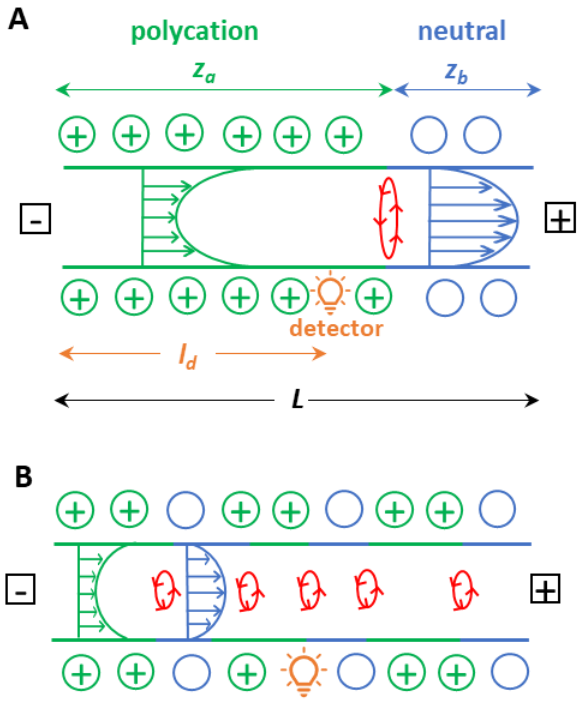

Figure 1. Impact of surface charge heterogeneity on velocity profiles in the capillary, in the case of a step discontinuity (A), and homogeneously distributed discontinuities (B).

First, the case of a flow pattern in CE with a step discontinuity in electroosmotic mobility was considered (Figure 1A). For a capillary column of length L and radius R with a step discontinuity in surface charge, hence in zeta potential and in electroosmotic mobility, the electroosmotic mobility of the first zone A of length z_a is noted $\mu_{eo,a}$, and that of the second zone B of length $L - z_a$, is noted $\mu_{eo,b}$. These electroosmotic mobilities correspond to electroosmotic velocities, $u_{eo,a}$ and $u_{eo,b}$ respectively. The variables denoted u represent cross-sectional averaged velocities, E is the applied electrical field and V the electrical potential drop

along the capillary. The mismatch between the electroosmotic velocities of the two zones generates, in each zone, a hydrodynamic Poiseuille-like flow to make up for this difference and insure the constancy of the mass flow-rate of the carrier liquid along the column (23,26). This hydrodynamic flow occurs in the direction of the overall flow in the zone with the lowest absolute value of the electroosmotic mobility and in the opposite direction in the other zone, as demonstrated in the fluorescence imaging experiments of Herr et al. (24) and in the numerical simulations of Lee et al. (27). The mean fluid mobility, μ_{eo}^0, within the capillary was shown to be equal to the length-averaged electroosmotic mobility (28):

$$\mu_{eo}^0 = f\mu_{eo,a} + (1-f)\mu_{eo,b} \quad (2)$$

with $f = \frac{z_a}{L}$ (3)

In each zone, the cross-sectional average value of the hydrodynamic component, $u_{hy,i}$, of the flow velocity can be expressed as:

$$u_{hy,a} = (1-f)\frac{V}{L}\Delta\mu_{eo} \quad (4)$$

$$u_{hy,a} = f\frac{V}{L}\Delta\mu_{eo} \quad (5)$$

with $\Delta\mu_{eo} = \mu_{eo,b} - \mu_{eo,a}$ (6)

For each zone *i (i=a,b)*, the velocity profile corresponds to the combination of a piston flow of magnitude $(\mu_{eo,i} + \mu_{ep})\frac{V}{L}$, where μ_{ep} is the analyte electrophoretic mobility, and a Poiseuille flow with mean velocity $u_{hy,i}$. The analyte plate height H_i in zone *i* is then:

$$H_i = \left(\frac{u_{hy,i}}{u_{app}}\right)^2 \frac{R^2 u_{app}}{24D} \quad (7)$$

where u_{app} is the apparent velocity of the analyte. Thus, in the case of a step discontinuity in zeta potential occurring after the detector ($z_a > l$) the apparent plate height H_{app}, defined as lm_2/m_1^2, where m_1 and m_2 are respectively the first moment and second central moment of the analyte residence time distribution recorded by the detector is given by:

$$H_{app} = (1-f)^2\left(\frac{\Delta\mu_{eo}}{\mu_{eo}^0+\mu_{ep}}\right)^2 \frac{R^2 u_{app}}{24D} \quad (8)$$

and if $z_a < l$, plate height can be expressed as:

$$H_{app} = F\left(\frac{\Delta\mu_{eo}}{\mu_{eo}^0+\mu_{ep}}\right)^2 \frac{R^2 u_{app}}{24D} \quad (9)$$

with $F = f\frac{L}{l} + f^2\left(1 - 2\frac{L}{l}\right)$ (10)

This result can then be generalized to a homogeneous ensemble of discontinuities (Figure 1B). Here, the situation where there is not a single discontinuity in surface charge, but a large number homogeneously distributed discontinuities between domains A and B is considered. Assuming that the system then behaves as if all zones A and all zones B were grouped together both before and after the detector position – a rather crude hypothesis – the plate height in this case would be obtained from Eq. 9 by writing $L/l = 1$ in Eq. 10, which gives:

$$H_{app} = f(1-f)\left(\frac{\Delta\mu_{eo}}{\mu_{eo}^0+\mu_{ep}}\right)^2 \frac{R^2 u_{app}}{24D} \quad (11)$$

Materials and Methods

Chemicals

2-[4-(2-hydroxyethyl)piperazin-1-yl]ethane sulfonic acid (HEPES) and acetic acid were purchased from Sigma-Aldrich (Saint-Quentin Fallavier, France). The model proteins, Carbonic Anhydrase I from human erythrocytes (CA, purity not indicated by the supplier), Myoglobin from equine skeletal muscle (Myo, purity ≥ 95%), Ribonuclease A from bovine pancreas (RNAse A, purity ≥ 60%), β-lactoglobulin A from bovine milk (β-lac A, purity ≥ 90%), and Lysozyme from chicken egg white (Lyz, purity ≥ 90%) were purchased from Sigma-Aldrich (Saint-Quentin Fallavier, France). Ultrapure water was obtained using a MilliQ system from Millipore (Molsheim, France). Poly(diallyldimethylammonium chloride) (PDADMAC, high molar mass: M_W 4 × 10^5 – 5 × 10^5 Da) 20% w/w in water was purchased from Aldrich (Lyon, France). Poly(styrene sulfonate) (PSS, M_W 7× 10^5 Da) was purchased from Acros Organics (Geel, Belgium). Poly(ethylene oxide) (PEO, M_W 1× 10^6 Da) was purchased from Sigma-Aldrich (Saint-Quentin Fallavier, France).

The BGE was 2 M acetic acid, pH 2.2, used for the inlet and outlet vials and for rinsing between runs. The construction buffer was a 20 mM HEPES solution with 10 mM NaOH, pH 7.4, used to rinse between polyelectrolyte layers. Polyelectrolyte solutions (3 gL^{-1} PDADMAC and PSS) were prepared in HEPES at least one night before the first use. PDADMAC solution must be kept in the freezer, as it was seen to degrade over time and lead to lower coating performance, and PSS solution in the fridge. PEO stock solution at 4 gL^{-1} in water was solubilized overnight and could be kept in the fridge several weeks. PEO coating solution at 2 gL^{-1} in 1.9 M NaCl, 0.1 M HCl was then prepared.

The protein mix to be analyzed was prepared from individual solutions of proteins in water at a higher concentration (2 gL^{-1}), as proteins degrade over time when stored in BGE and may interact with each other if stored together (26). These stock solutions could be kept in the freezer for several months. To prepare the sample before analysis, they were thawed and 10 µL of each one were combined, adding another 50 µL of 4M AcOH for a final 100 µL aliquot with each protein at 0.2 gL^{-1} in 2M AcOH. This solution underwent a heat treatment at 37°C for 30 min and was added to a polypropylene conical vial for analysis. The rest of the aliquot may be kept in the freezer for a short period of time. 0.002% DMF in BGE was used as the EOF marker and injected before the proteins.

Coating Procedures

The normal SMIL coatings were prepared by flushing the silica capillary with 1 M NaOH for 10 min, then with water for 5 min and HEPES for 10 min. Next, the polyelectrolyte solutions were flushed for 7 min each, followed by 3 min of HEPES, starting with the polycation and alternating with the polyanion, for a total of 5 layers. After the last HEPES flush, wait 5 min and flush with water for 3 min, with BGE for 10 min and wait for another 5 min before starting analyses. All flushes were performed at 930 mbar. Different

HEPES vials were used after the polycation and the polyanion in order to limit cross-contamination.

Partial PDADMAC on PEO coatings were prepared following a protocol by Danger et al. (29). First, PEO coatings were prepared by rinsing the capillary with high pressure flushes at 2.8 bar (adjusted to the capillary length): 2 min with water, 5 min with HCl 1M, 10 min with PEO solution, and 2 min with water. Then, the capillary was flushed with HEPES for 3 min at 930 mbar and with PDADMAC at 50 mbar for a duration t_{inj} (see details below). To evacuate the PDADMAC solution and ensure only partial coating of the capillary, it was then flushed with HEPES at 100 mbar for 20 min from the outlet side, applying a negative pressure on the Agilent CE instrument. Then, wait for 5 min, flush normally with water for 3 min, BGE for 5 min, and wait 5 min before analysis.

To calculate the duration of the PDADMAC rinse, the viscosity of the HEPES and PDADMAC solutions must be determined. Indeed, the injected volume is linked to injection time and pressure as well as viscosity, and in this case, PDADMAC solution was injected while the capillary was filled with HEPES, thus both viscosities come into play. Viscosities were determined by injecting DMF in each solution (HEPES and PDADMAC) as a front and comparing the times corresponding to the inflection point of the curve with the one given by DMF in water, knowing the viscosity of water at 25°C (30). Then, the injected volume may be calculated with the following equation established by Danger et al. (29):

$$V_x = \frac{\pi R^2 L \eta_{el}}{\eta_{sol} - \eta_{el}} \left[-1 + \sqrt{\frac{R^2 \Delta P t_{inj} (\eta_{sol} - \eta_{el})}{4 L^2 \eta_{el}^2}} \right] \quad (12)$$

where V_x is the injected volume, η_{sol} the PDADMAC viscosity, η_{el} the HEPES viscosity, ΔP the injection pressure, and t_{inj} the injection time.

So, for a capillary 90% coated with PDADMAC and 10% with PEO, we can set $V_x = 0.9\ V_{cap}$, where V_{cap} is the volume of the capillary, leading to the determination of t_{inj}. The results were as follows: η_{HEPES} = 1.01 $\times 10^{-3}$ Pa.s, $\eta_{PDADMAC}$ = 1.29 $\times 10^{-3}$ Pa.s, t_{inj} = 943 s at ΔP = 50 mbar for a 60 cm, 50 µm I.D. capillary. A low pressure was chosen for better precision. It should be noted that like PEO coatings, the partial PDADMAC-PEO coatings needed to be regenerated every 5 runs to ensure stable EOF, and so the following high pressures flushes at 3 bar were implemented every 5 runs: NaOH for 5 min, HCl for 5 min, BGE for 5 min, followed by the previously described PEO and partial PDADMAC coating procedures.

Capillary Electrophoresis

Analyses were performed on an Agilent 7100 CE in a 2 M acetic acid BGE at pH 2.2. Fused silica capillaries of 50 µm in diameter and 60 cm total length (51.5 cm to the detector) were used. Applied voltages were typically between -30kV and -10kV. The capillary was flushed for 5 min with BGE before each run. A 0.002% solution of DMF in BGE was injected first as the EOF marker (30 mbar, 3 s), and the protein mixture next (30 mbar, 6 s), with CA, Myo, RNAse A, β-lac A and Lyz each at 0.2 g/L in BGE. The temperature was set at 25°C and detection wavelength was 214 nm.

Calculations of separation efficiencies were done with CEval software (31) available at [https://echmet.natur.cuni.cz/]. The capillary total (L) and effective (l) lengths must be entered in the software, as well as the half ramp time ($t_{1/2}$ = 0.6 s on Agilent instruments).

AFM lithography measurements

AFM lithography measurements have been performed to determine the thickness of each layer. Several images of each layer have been recorded to statistically relevant evaluate the roughness. AFM nanolithography was done by increasing the force in contact mode in selected small areas (500 x 500nm^2) to remove surface-bound molecules. Therefore 10 fast scans were done at a scan rate > 20 lines/s at reduced feedback parameters using forces typically > 20nN, followed by a 3 µm^2 scan using former imaging parameters. The layer thickness was determined by cross-section analysis.

Simultaneous topography and recognition imaging (TREC)

For TREC measurements, Bruker MSCT cantilevers (Bruker, USA) have been bio-functionalized with avidin following an established protocol (32). TREC measurements have been performed using a Keysight 5500 SPM 1 AFM with TREC box (Keysight, Santa Barbara). Tip functionalization has been proven by performing adhesion force spectroscopy (32) on differently charged surfaces, e.g. freshly cleaved mica showing adhesion and freshly prepared avidin surface showing no adhesion. All AFM images have been evaluated using Gwyddion software.

Results and discussion

Questioning the theory of equilibrium adsorption

Previous studies showed that SMIL coatings composed of PDADMAC and PSS in an acetic acid BGE led to excellent repeatability, reproducibility and separation efficiency (26). However, even in such optimized conditions, plate height increased with the electric field, limiting the possibility of working at high voltages:

$$H = \frac{2D}{u} + pu + constant \quad (13)$$

where D is the diffusion coefficient, u the solute linear velocity and p the slope. The first term is due to axial diffusion and the second to the resistance to mass transfer in the mobile phase, while the constant includes extra-column effects such as injection, detection or electromigration dispersion.

The slope was interpreted as solute adsorption with a rapid exchange and modelized with the following equation as a function of the retention factor k:

$$H = \frac{2D}{u(1+k)} + \frac{{d_c}^2 u}{D}\frac{k^2}{16(1+k)} + constant \qquad (14)$$

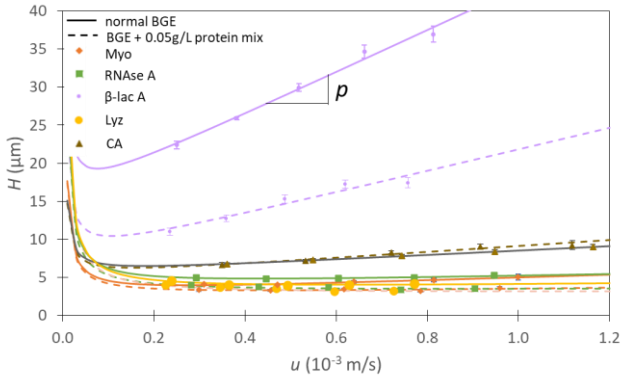

Figure 2. *H vs u* representations for the separation of five model basic proteins on a 5-layer PDADMAC/PSS SMIL coating, in normal BGE (full lines) and BGE containing 0.01g/L of each protein (dashed lines). CA in brown, Myo in orange, RNAse A in green, β-lac A in purple, Lyz in yellow. Error bars are ± one SD on *n*=5 repetitions. Experimental conditions: 5-layer SMIL coated capillary terminating with the polycation PDADMAC. Capillary: 60 cm (51.5 cm to the detector) x 50 µm I.D. BGE: 2 M acetic acid, pH 2.2. Flush before each run: BGE 1 bar, 5 min. Hydrodynamic injection: 30 mbar, 6 s. Sample mixture: 0.2 g/L of each protein in BGE. Hydrodynamic co-injection of 0.002% DMF in BGE: 30 mbar, 3 s. Temperature: 25°C. For the coating procedure, see section 2.2. For the analyses in BGE containing the protein mixture (0.01 g/L of each protein), CA: $p(10^{-3}\ s)$ = 4.00 ± 0.45; Myo: $p(10^{-3}\ s)$ = 0.73 ± 0.17; RNAse A: $p(10^{-3}\ s)$ = 0.30 ± 0.48, β-lac A: $p(10^{-3}\ s)$ = 14.27 ± 1.98; Lyz: $p(10^{-3}\ s)$ = 0.22 ± 0.45.

Thus, this equation allows calculating retention factors of analytes on the capillary coating, estimating residual adsorption and giving access to a ranking of different capillary coating performances.

This model was applied in this work to the separation of a mix of 5 model proteins (CA, Myo, RNAse A, β-lac A, Lyz) on a 5-layer PDADMAC/PSS SMIL in 2 M acetic acid BGE, leading to the *H vs u* curves shown in Figure 2. Both the slopes *p* and the resulting retention factors *k* were calculated, as well as the constants and plate numbers (see Table 1). The much higher slope of β-lac A, 5 to 10 times larger compared to the other proteins, indicates either a much larger retention of the protein onto the capillary wall or the presence of an additional source of dispersion.

In order to confirm the theory of equilibrium adsorption of proteins onto the capillary wall, these results were confronted with Taylor dispersion analysis (TDA) experiments performed in identical conditions to CE. For that, each protein was injected individually with 0.002% DMF, and transported along the capillary by an applied pressure of 50 mbar. Figure 3 shows the signal obtained from the injection of β-lac A at 1 g/L containing 0.002% DMF. This signal was fitted with two Gaussians that correspond to the two injected species, β-lac A and DMF, which elute at the same time t_0 = 14.1 min. If the protein was retained, as expected from the model used in Figure 2, a retention time of t_r = 15.8 min should have been observed for β-lac A as displayed in Figure 3 (dashed line), and corresponding to $k(10^{-2})$ = 12.20 ± 0.31. Hence, we can conclude that there is no fast kinetics interaction of β-lac A onto the capillary surface, as described by the previous model. The same conclusion can be drawn for the other proteins. For β-lac A, if there is indeed adsorption contributing to *p*, it must be a process which involves few interacting sites and slow kinetics of desorption, resulting in a non-retardation of the peak apex.

Table 1. Values of *H vs u* slopes *p*, retention factors *k*, constants and number of theoretical plates at -15kV for 5 model proteins separated on a 5-layer PDADMAC/PSS SMIL in 2M acetic acid. Other experimental conditions as in Figure 1.

	$p\ (10^{-3}\ s)$	*cst* (µm)	$N\ (10^3)$ at -15kV	$k\ (10^{-2})$
CA	4.36 ± 0.31	3.76 ± 0.24	82.2	3.73 ± 0.13
Myo	2.96 ± 0.05	1.78 ± 0.03	148.4	3.79 ± 0.03
RNAse A	2.22 ± 0.20	2.52 ± 0.08	128.9	4.09 ± 0.18
β-lac A	25.35 ± 1.25	5.83 ± 0.61	33.3	12.20 ± 0.31
Lyz	2.71 ± 0.08	1.38 ± 0.04	167.9	4.89 ± 0.09

Adsorption with slow kinetics of desorption and a low number of interacting sites as a source of dispersion

Adsorption with slow kinetics has been studied in the literature, namely by Ermakov et al., who pointed out that the adsorption process is controlled by wall capacity and interaction kinetics between the solute and the wall (33). Similarly, Schure and Lehnhoff cited sorption and desorption kinetics as some of the factors governing peak broadening, and demonstrated that resolution worsens when they are slow (34). In addition to kinetics, the number of adsorption sites also has its importance, since more adsorption sites compared to the injected amount leads to broader peaks (6).

A way of validating the theory of adsorption involving slow kinetics and a small number of interacting sites consists in saturating the adsorption sites. For that, a small amount (0.01 g/L) of each protein was added to the BGE which should saturate the available sites and lead to reduced adsorption of the considered protein. Figure 2 (see dotted lines) shows that the slopes of CA, Myo, RNAse A and Lyz did not vary much when the protein mix was added to the BGE compared to the BGE without protein, whereas the slope of β-lac A decreased significantly (almost by a factor

2), confirming that the capillary coating is sensible to saturation for that protein. Adding more protein to the BGE did not have the effect of lowering the slope further, demonstrating the small binding capacity of the capillary coating, which was saturated even with a very low concentration of proteins.

In addition, rinsing the capillary with the protein mix before the analyses in a normal BGE also led to a decreased β-lac A slope, confirming that the adsorption that takes place has slow kinetics (see Figure SI1). Hence, we can conclude that p in the case of β-lac A is, at least in part, due to adsorption with slow kinetics and few adsorption sites. β-lac A's susceptibility to this type of adsorption may be linked to its nature. Indeed, a study using Monte Carlo simulation revealed that β-lactoglobulin interacts with strong polycations resulting in complex formation (35). Such an effect could explain the higher slope of β-lac A compared to the other proteins.

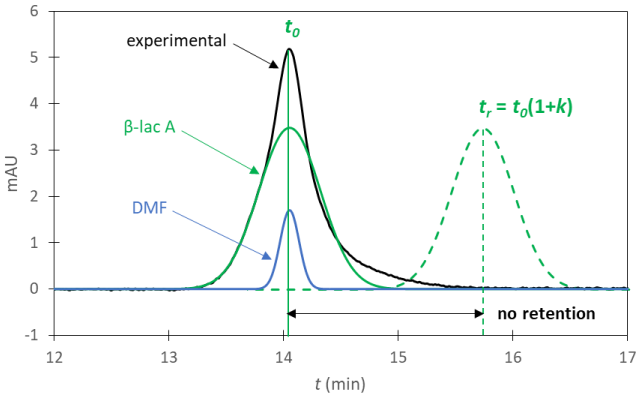

Figure 3. TDA of β-lactoglobulin A (green Gaussian) injected with DMF (blue Gaussian) in BGE fitted by two Gaussian curves. Experimental curve in black, 2-Gaussian fit in red, Gaussian 1 in green and Gaussian 2 in blue. Experimental conditions: 5-layer SMIL coated capillary terminating with the polycation PDADMAC. Capillary: 60 cm (51.5 cm to the detector) x 50 µm I.D. BGE: 2 M acetic acid, pH 2.2. Flush before run: BGE 1 bar, 5 min. Hydrodynamic injection: 30 mbar, 6 s. Mobilization pressure: 50 mbar. Sample mixture: 1 g/L of β-lac A with 0.002% DMF in AcOH 2M Temperature: 25°C. For the coating procedure, see section 2.2

However, an explication for the slopes of the other model proteins needs to be found, as they are not sensitive to saturation. Moreover, experiments done on small molecules which are assumed to not be adsorbed onto the capillary coating also led to a slope in the *H vs u* curves, indicating that there is another contribution to the slope that is not due to adsorption (see Figure SI2).

Demonstrating the impact of electroosmotic inhomogeneity using partial capillary coatings

One hypothesis to explain the low values of p observed for CA, Myo, RNAse A and Lyz is that heterogeneities in the coating lead to local variations in electroosmotic mobilities, contributing to peak dispersion. An expression giving the plate height in CE when there is a discontinuity in electroosmotic mobility along the capillary was established (see Theoretical Part). In order to validate these equations, inhomogeneous coatings were intentionally prepared according to a method proposed by Danger et al (29), whereby polyelectrolytes were deposited on sections of the capillary surface, producing a non-uniform surface charge distribution, in a process similar to that of Herr et al. (24). The protocol is based on the deposition of a polycationic PDADMAC layer onto a previously deposited neutral PEO layer all along the capillary.

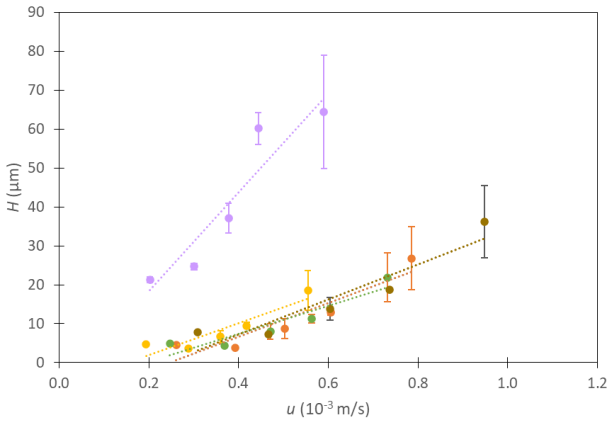

Figure 4. *H vs u* representations for the separation of five model proteins on a partial 90% PDADMAC on PEO coating. CA in brown, Myo in orange, RNAse A in green, β-lac A in purple, Lyz in yellow. Error bars are ± one SD on n=5 repetitions. Other experimental conditions as in Figure 1. CA: $p(10^{-3}$ s) = 45.09 ± 9.81, Myo: $p(10^{-3}$ s) = 43.45 ± 9.72, RNAse A: $p(10^{-3}$ s) = 35.91 ± 8.12, β-lac A: $p(10^{-3}$ s) = 127.10 ± 27.33, Lyz: $p(10^{-3}$ s) = 40.50 ± 10.31.

Previous experiments showed that PEO coated capillaries required regeneration every 5 runs in order to maintain a stable EOF (results not shown). Thus, the full procedure (PEO coating and partial PDADMAC coating) was also repeated every 5 runs for better accuracy (see experimental section 2.2). The usual series of protein separations at different voltages, between -30 and -10kV, was carried out and the *H vs u* curves were plotted (see the corresponding electropherograms in Figure SI3). Despite larger error bars compared to SMIL coatings, Figure 4 shows a significant increase in p for all proteins, with a value of p (in 10^{-3} s) = 41.2 ± 4.0 on average for the four model proteins CA, Myo, RNAse A and Lyz compared to an average p (in 10^{-3} s) = 3.06 ± 0.92 on a 5-layer PDADMAC/PSS SMIL, while p (in 10^{-3} s) = 127 ± 27 compared to p (in 10^{-3} s) = 25.3 ± 1.2 for β-lac A. From these values, it is possible to use Eq. 8 for a step discontinuity in the case $z_a > l$ to estimate the fraction of the capillary length coated by the PDADMAC layer. Taking CA as example, and knowing that $\Delta\mu_{eo} = \mu_{eo,PEO} - \mu_{eo,PDADMAC} = 0.2 - (-46.0) = 46.2$ TU, mean μ_{eo}^{0}= -41.9 TU, D = 4.81 ×10^{-11} m^2s^{-1}, p (in 10^{-3} s) = 45.1, Eq. (8) led to f= 0.89. The same procedure was applied to Myo, RNAse A and Lyz, giving an average value of 0.88 ± 0.02, which is very close to the intended value of 0.9.

The same model was next applied to the 5-layer SMIL coating as a way to estimate surface charge inhomogeneity using the homogeneous discontinuity equation (Eq. 11). Figure 5 shows that on a 5-layer PDADMAC/PSS SMIL coating, even a very low fraction of inhomogeneity *f* generates a substantial increase in *p*. Indeed, the experimental slope of CA on such a coating is worth 4.36×10^{-3} s , which corresponds to about 0.2% inhomogeneity if we consider that the coating is made up of polycationic (PDADMAC) zones and neutral zones ($\Delta\mu_{eo} \approx 48$ TU) and about 0.4% if we consider that it is made up of polycationic (PDADMAC) and polyanionic (PSS) zones ($\Delta\mu_{eo} \approx 80$ TU). The other proteins led to similar results (see Figure SI4). On one

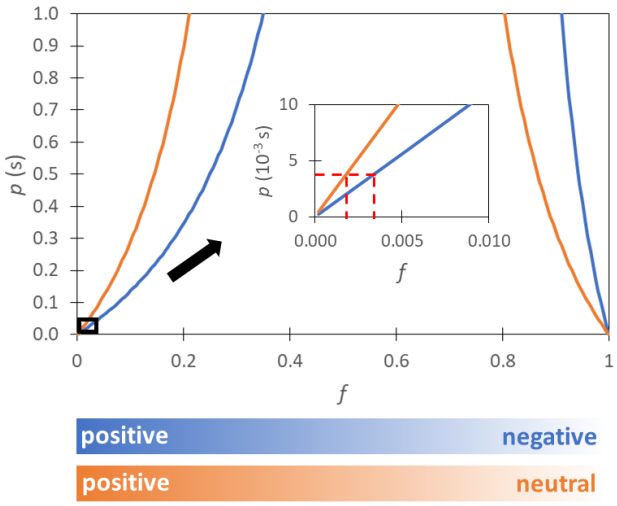

hand, the case of positive and negative zones could correspond to holes in the final PDADMAC layer which let through the negatively charged PSS below. On the other hand, the case of the positive and neutral zones could illustrate alternations on the surface of the SMIL between an excess of PDADMAC (due to uncompensated polyelectrolyte loops) and more or less neutral zones where a compensation between PDADMAC and PSS charges occurs.

Figure 5. Variation of the slope p of the *H vs u* curve with the fraction *f* of coating inhomogeneities as given by Eq. 11 for CA. The blue curve corresponds to the case of positive (PDADAMAC) and negative (PSS) zones ($\Delta\mu_{eo} \approx 80$ TU), and the orange curve to the case of positive (PDADAMAC) and neutral (compensated PDADMAC/PSS) ($\Delta\mu_{eo} \approx 48$ TU). In the insert the curves are zoomed to show the *f* range corresponding to the observed experimental *p* value.

The model taking into account electroosmotic inhomogeneity demonstrates that even a very low amount of charge heterogeneity of the coating leads to increased dispersion as the electric field increases, providing a more accurate understanding of the factors limiting the separation efficiency.

Backing the model with TREC-AFM data

To illustrate coating homogeneity, it is interesting to use imaging techniques such as AFM and TREC. AFM has been applied to the characterization of various coatings in CE, both on glass slides (8,36,37) and directly inside cut capillaries 8-40). In addition to topography, charge distribution may also be evaluated using TREC, in which the AFM tip is modified with a protein acting as a biosensor, leading to adhesion maps (32,41). In the current work, both AFM and TREC were conducted on $(PDADMAC/PSS)_{2.5}$ coatings reproduced on glass slides using avidin as the biosensor in order to try to visualize the charge inhomogeneity discussed in the previous section.

The thickness measurements, shown in Table 2, are in accordance with results found with a quartz microbalance (QCM) for the same coating (42). Cleaning the initial glass surface with piranha solution or SDS, isopropanol, and water was essential to remove impurities. The final 5-layer coating had a very low roughness compared to other SMILs studied in the literature (Rms 1.43 nm for a $(PDADMAC/DS)_{1.5}$55% poly(acrylamide-co2-acrylamido-2-methyl-1-propansulfonate) $(PAMAMPS)_1$ SMIL) (32,41). The topography image given by the TREC in Figure 6 also shows very few variations in height which corresponds to the low Rms values. Thus, it seems to form a thin, rigid film with a low level of hydration. The roughness can be interpreted as the presence of loops formed by entangled polymer segments.

Table 2. Roughness and thickness of each layer of a $(PDADMAC/PSS)_{2.5}$ SMIL determined by AFM.

Layer	Rms (nm) (full image)	Rms (nm) (average over 5 parts)	Thickness of the scratch (nm) (over 5 cross sections)
Glass	0.78	0.79 ± 0.06	
1	0.25	0.25 ± 0.03	0.58 ± 0.06
2	0.37	0.35 ± 0.03	1.44 ± 0.32
3	0.49	0.48 ± 0.01	2.01 ± 0.22
4	0.65	0.41 ± 0.06	3.81 ± 0.23
5	0.37	0.28 ± 0.10	5.91 ± 0.57

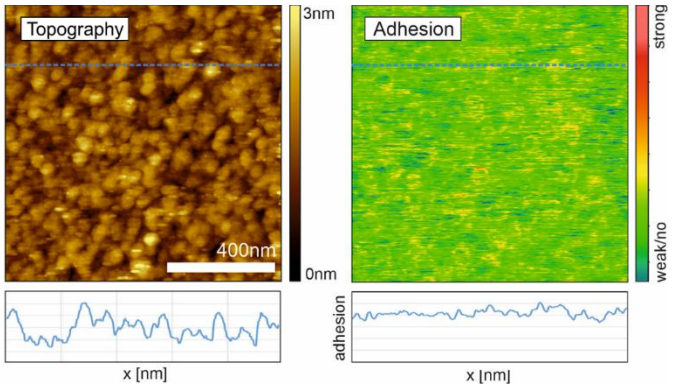

Figure 6. AFM and TREC imaging of a $(PDADMAC/PSS)_{2.5}$ SMIL.

The TREC adhesion images indicate that the $(PDADMAC/PSS)_{2.5}$ SMIL is very homogeneous in charge as avidin shows no interaction with the surface (see Figure

6). The few signals observed likely correspond to noise and topography crosstalk. As presented in the previous section, very low heterogeneity, less than 1%, was expected, which could be difficult to visualize using TREC. One explanation could be that, unlike hypothesized in the model, the charge heterogeneity is not homogeneously distributed along the capillary but is concentrated to one area, making it challenging to observe with just a few measurements. Another possibility is that the charge difference between the heterogeneous zones is too small to be detected in TREC, meaning that the slopes *p* are intrinsic to the SMIL.

The link between coating heterogeneity and separation efficiency may be extended to fused silica capillaries, which were previously shown to result in much higher retention factors, and therefore slopes in the *H vs u* curves, compared to SMIL coated capillaries (1). In view of the present results, this poor separation efficiency is likely due to electroosmotic inhomogeneity resulting from protein adsorption onto the capillary surface.

Conclusion

In this work, different sources of dispersion occurring during protein separation by CE using SMIL coatings were investigated. To this end, a mix of model proteins was separated using $(PDADMAC/PSS)_{2.5}$ coatings in 2 M acetic acid BGE, and *H vs u* profiles were determined. The model of rapid-exchange adsorption was finally found to be unsuitable since TDA experiments in identical experimental conditions did not show any retention of the proteins on the capillary coating. It was demonstrated that the slope *p* can be explained by charge heterogeneity of the coating generating EOF irregularities and thus peak dispersion, and for some proteins, such as β-lac A, by adsorption with slow kinetics of desorption. It is worth noting that the validity of the model giving the *H vs u* dependence in the case of rapid-exchange adsorption is not in question, it is its applicability and relevance for describing peak broadening in CE that is challenged, at least for SMIL coatings. As demonstrated in the case of TDA, adsorption phenomena in CE are more relevantly described by interactions with a low number of interacting sites and slow kinetics of desorption. This was proved in this work by conducting separations in BGE containing proteins, which saturated the available sites, showing that such mechanisms contribute to plate height for some proteins. All in all, a better understanding of the factors influencing peak dispersion in CE was obtained. Regarding SMIL coatings, it seems that the relatively low residual slope ($p \approx 3 \times 10^{-3}$ s) in the *H vs u* profiles is inherently due to residual surface charge heterogeneity that can be very difficult to eliminate. Still, the $(PDADMAC/PSS)_{2.5}$ coating remains a very robust and efficient coating for CE of proteins and other macrobiomolecules.

ASSOCIATED CONTENT

Supporting Information

Supplementary material associated with this article can be found in the online version. Theoretical part about plate height in CE with a discontinuity in electroosmotic mobility. *H vs u* curves after presaturation of the capillary coating by the protein mix. H vs u curves for three small molecules on a SMIL coating. Electropherograms on a PDADMAC-PEO coated capillary. Determination of SMIL inhomogeneity for different model proteins.

AUTHOR INFORMATION

Corresponding Author

Hervé Cottet. Phone: +33 4 67 14 34 27. Fax: +33 4 67 63 10 46. E-mail: herve.cottet@umontpellier.fr. ORCID Hervé Cottet: 0000-0002-6876-175X

Author Contributions

The manuscript was written through contributions of all authors.

ACKNOWLEDGMENT

This work was done as part of a PRCI in collaboration with German partners from the University of Aalen, Germany (ANR-DFG SMIL E, ANR-20-C E 92-0021-01) as well as the Institute of Biophysics, Johannes Kepler University Linz.

REFERENCES

(1) Leclercq, L.; Renard, C.; Martin, M.; Cottet, H. Quantification of Adsorption and Optimization of Separation of Proteins in Capillary Electrophoresis. *Anal. Chem.* **2020**, *92* (15), 10743–10750. https://doi.org/10.1021/acs.analchem.0c02012.

(2) Regnier, F. E.; Wu, D. Capillary Electrophoresis Technology. In *Capillary Electrophoresis Technology*; Chromatographic science series; Marcel Dekker, New York, 1993; pp 287–309.

(3) Minárik, M.; Gaš, B.; Rizzi, A.; Kenndler, E. Plate Height Contribution from Wall Adsorption in Capillary Zone Electrophoresis of Proteins. *J. Capillary Electrophor.* **1995**, *2* (2), 89–96.

(4) Kenndler, E. Capillary Zone Electrophoresis in the Absence of Electroosmotic Flow. In *High-Performance Capillary Electrophoresis*; 1998; Vol. 146, pp 34–53.

(5) Hajba, L.; Guttman, A. Recent Advances in Column Coatings for Capillary Electrophoresis of Proteins. *TrAC, Trends Anal. Chem.* **2017**, *90*, 38–44. https://doi.org/10.1016/j.trac.2017.02.013.

(6) Lucy, C. A.; MacDonald, A. M.; Gulcev, M. D. Non-Covalent Capillary Coatings for Protein Separations in Capillary Electrophoresis. *J. Chromatogr. A* **2008**, *1184* (1–2), 81–105. https://doi.org/10.1016/j.chroma.2007.10.114.

(7) Melanson, J. E.; Baryla, N. E.; Lucy, C. A. Double-Chained Surfactants for Semipermanent Wall Coatings in Capillary Electrophoresis. *Anal. Chem.* **2000**, *72* (17), 4110–4114. https://doi.org/10.1021/ac000335z.

(8) Baryla, N. E.; Lucy, C. A. Semi-Permanent Surfactant Coatings for Inorganic Anion Analysis in Capillary Electrophoresis. *J. Chromatogr. A* **2002**, *956* (1–2), 271–277. https://doi.org/10.1016/S0021-9673(01)01516-3.

(9) Yassine, M. M.; Lucy, C. A. Factors Affecting the Temporal Stability of Semipermanent Bilayer Coatings in Capillary Electrophoresis Prepared Using Double-Chained Surfactants. *Anal. Chem.* **2004**, *76* (11), 2983–2990. https://doi.org/10.1021/ac035372f.

(10) Wang, C.; Lucy, C. A. Mixed Cationic/Anionic Surfactants for Semipermanent Wall Coatings in Capillary Electrophoresis. *Electrophoresis* **2004**, *25* (6), 825–832. https://doi.org/10.1002/elps.200305760.

(11) Wang, C.; Lucy, C. A. Oligomerized Phospholipid Bilayers as Semipermanent Coatings in Capillary Electrophoresis. *Anal. Chem.* **2005**, *77* (7), 2015–2021. https://doi.org/10.1021/ac0489622.

(12) Katayama, H.; Ishihama, Y.; Asakawa, N. Stable Cationic Capillary Coating with Successive Multiple Ionic Polymer Layers for Capillary Electrophoresis. *Anal. Chem.* **1998**, *70* (24), 5272–5277. https://doi.org/10.1021/ac980522l.

(13) Xuan, X.; Li, D. Band-Broadening in Capillary Zone Electrophoresis with Axial Temperature Gradients. *Electrophoresis* **2005**, *26* (1), 166–175. https://doi.org/10.1002/elps.200406141.

(14) Malá, Z.; Gebauer, P.; Boček, P. New Methodology for Capillary Electrophoresis with ESI-MS Detection: Electrophoretic Focusing on Inverse Electromigration Dispersion Gradient. High-Sensitivity Analysis of Sulfonamides in Waters. *Anal. Chim. Acta* **2016**, *935*, 249–257. https://doi.org/10.1016/j.aca.2016.06.016.

(15) Kašička, V.; Prusík, Z.; Gaš, B.; Štědrý, M. Contribution of Capillary Coiling to Zone Dispersion in Capillary Zone Electrophoresis. *Electrophoresis* **1995**, *16* (1), 2034–2038. https://doi.org/10.1002/elps.11501601332.

(16) Bullock, J. Application of Capillary Electrophoresis to the Analysis of the Oligomeric Distribution of Polydisperse Polymers. *J. Chromatogr. A* **1993**, *645* (1), 169–177. https://doi.org/10.1016/0021-9673(93)80631-H.

(17) Gaš, B.; Kenndler, E. Dispersive Phenomena in Electromigration Separation Methods. *Electrophoresis* **2000**, *21* (18), 3888–3897. https://doi.org/10.1002/1522-2683(200012)21:18<3888::AID-ELPS3888>3.0.CO;2-D.

(18) Ghosal, S. Fluid Mechanics of Electroosmotic Flow and Its Effect on Band Broadening in Capillary Electrophoresis. *Electrophoresis* **2004**, *25* (2), 214–228. https://doi.org/10.1002/elps.200305745.

(19) Khodabandehloo, A. Size Characterization of Particles Using Capillary Electrophoresis. PhD Thesis, University of British Columbia, 2018. https://doi.org/10.14288/1.0365261.

(20) Griffiths, S. K.; Nilson, R. H. Electroosmotic Fluid Motion and Late-Time Solute Transport for Large Zeta Potentials. *Anal. Chem.* **2000**, *72* (20), 4767–4777. https://doi.org/10.1021/ac000539f.

(21) Zholkovskij, E. K.; Masliyah, J. H.; Czarnecki, J. Electroosmotic Dispersion in Microchannels with a Thin Double Layer. *Anal. Chem.* **2003**, *75* (4), 901–909. https://doi.org/10.1021/ac0203591.

(22) Ajdari, A. Electro-Osmosis on Inhomogeneously Charged Surfaces. *Phys. Rev. Lett.* **1995**, *75* (4), 755–758. https://doi.org/10.1103/PhysRevLett.75.755.

(23) Long, D.; Stone, H. A.; Ajdari, A. Electroosmotic Flows Created by Surface Defects in Capillary Electrophoresis. *J. Colloid Interface Sci.* **1999**, *212* (2), 338–349. https://doi.org/10.1006/jcis.1998.6015.

(24) Herr, A. E.; Molho, J. I.; Santiago, J. G.; Mungal, M. G.; Kenny, T. W.; Garguilo, M. G. Electroosmotic Capillary Flow with Nonuniform Zeta Potential. *Anal. Chem.* **2000**, *72* (5), 1053–1057. https://doi.org/10.1021/ac990489i.

(25) Towns, J. K.; Regnier, F. E. Impact of Polycation Adsorption on Efficiency and Electroosmotically Driven Transport in Capillary Electrophoresis. *Anal. Chem.* **1992**, *64* (21), 2473–2478. https://doi.org/10.1021/ac00045a003.

(26) Dhellemmes, L.; Leclercq, L.; Höchsmann, A.; Neusüß, C.; Biron, J.-P.; Roca, S.; Cottet, H. Critical Parameters for Highly Efficient and Reproducible Polyelectrolyte Multilayer Coatings for Protein Separation by Capillary Electrophoresis. *J. Chromatogr. A* **2023**, *1695*, 463912. https://doi.org/10.1016/j.chroma.2023.463912.

(27) Lee, J. S. H.; Ren, C. L.; Li, D. Effects of Surface Heterogeneity on Flow Circulation in Electroosmotic Flow in Microchannels. *Anal. Chim. Acta* **2005**, *530* (2), 273–282. https://doi.org/10.1016/j.aca.2004.09.026.

(28) Anderson, J. L.; Keith Idol, W. Electroosmosis Through Pores With Nonuniformly Charged Walls. *Chem. Eng. Commun.* **1985**, *38* (3–6), 93–106. https://doi.org/10.1080/00986448508911300.

(29) Danger, G.; Pascal, R.; Cottet, H. Non-Uniform Surface Charge Distributions in CE: Theoretical and Experimental Approach Based on Taylor Dispersion. *Electrophoresis* **2008**, *29* (20), 4226–4237. https://doi.org/10.1002/elps.200800128.

(30) Bello, M. S.; Rezzonico, R.; Righetti, P. G. Capillary Electrophoresis Instrumentation as a Bench-Top Viscometer. *J. Chromatogr. A* **1994**, *659* (1), 199–204. https://doi.org/10.1016/0021-9673(94)85022-4.

(31) Dubský, P.; Ördögová, M.; Malý, M.; Riesová, M. CEval: All-in-One Software for Data Processing and Statistical Evaluations in Affinity Capillary Electrophoresis. *J. Chromatogr. A* **2016**, *1445*, 158–165. https://doi.org/10.1016/j.chroma.2016.04.004.

(32) Leitner, M.; Stock, L. G.; Traxler, L.; Leclercq, L.; Bonazza, K.; Friedbacher, G.; Cottet, H.; Stutz, H.; Ebner, A. Mapping Molecular Adhesion Sites inside SMIL Coated Capillaries Using Atomic Force Microscopy Recognition Imaging. *Anal. Chim. Acta* **2016**, *930*, 39–48. https://doi.org/10.1016/j.aca.2016.05.002.

(33) Ermakov, S. V.; Zhukov, M. Yu.; Capelli, L.; Righetti, P. G. Wall Adsorption in Capillary Electrophoresis Experimental Study and Computer Simulation. *J. Chromatogr. A* **1995**,

699 (1–2), 297–313. https://doi.org/10.1016/0021-9673(94)01228-7.

(34) Schure, M. R.; Lenhoff, A. M. Consequences of Wall Adsorption in Capillary Electrophoresis: Theory and Simulation. *Anal. Chem.* **1993**, *65* (21), 3024–3037. https://doi.org/10.1021/ac00069a015.

(35) Torres, P.; Bojanich, L.; Sanchez-Varretti, F.; Ramirez-Pastor, A. J.; Quiroga, E.; Boeris, V.; Narambuena, C. F. Protonation of β-Lactoglobulin in the Presence of Strong Polyelectrolyte Chains: A Study Using Monte Carlo Simulation. *Colloids and Surfaces B: Biointerfaces* **2017**, *160*, 161–168. https://doi.org/10.1016/j.colsurfb.2017.09.018.

(36) Haselberg, R.; Flesch, F. M.; Boerke, A.; Somsen, G. W. Thickness and Morphology of Polyelectrolyte Coatings on Silica Surfaces before and after Protein Exposure Studied by Atomic Force Microscopy. *Anal. Chim. Acta* **2013**, *779*, 90–95. https://doi.org/10.1016/j.aca.2013.03.066.

(37) Horvath, J.; Dolník, V. Polymer Wall Coatings for Capillary Electrophoresis. *Electrophoresis* **2001**, *22* (4), 644–655. https://doi.org/10.1002/1522-2683(200102)22:4<644::AID-ELPS644>3.0.CO;2-3.

(38) Bonvent, J. J.; Barberi, R.; Bartolino, R.; Capelli, L.; Righetti, P. G. Adsorption of Proteins to Fused-Silica Capillaries as Probed by Atomic Force Microscopy. *J. Chromatogr. A* **1996**, *756* (1–2), 233–243. https://doi.org/10.1016/S0021-9673(96)00631-0.

(39) Cifuentes, A.; Díez-Masa, J. C.; Fritz, J.; Anselmetti, D.; Bruno, A. E. Polyacrylamide-Coated Capillaries Probed by Atomic Force Microscopy: Correlation between Surface Topography and Electrophoretic Performance. *Anal. Chem.* **1998**, *70* (16), 3458–3462. https://doi.org/10.1021/ac9801420.

(40) Barberi, R.; Giocondo, M.; Bartolino, R.; Righetti, P. G. Probing the Inner Surface of a Capillary with the Atomic Force Microscope. *Electrophoresis* **1995**, *16* (1), 1445–1450. https://doi.org/10.1002/elps.11501601239.

(41) Stock, L. G.; Leitner, M.; Traxler, L.; Bonazza, K.; Leclercq, L.; Cottet, H.; Friedbacher, G.; Ebner, A.; Stutz, H. Advanced Portrayal of SMIL Coating by Allying CZE Performance with In-Capillary Topographic and Charge-Related Surface Characterization. *Anal. Chim. Acta* **2017**, *951*, 1–15. https://doi.org/10.1016/j.aca.2016.10.030.

(42) Roca, S.; Leclercq, L.; Gonzalez, P.; Dhellemmes, L.; Boiteau, L.; Rydzek, G.; Cottet, H. Modifying Last Layer in Polyelectrolyte Multilayer Coatings for Capillary Electrophoresis of Proteins. *J. Chromatogr. A* **2023**, *1692*, 463837. https://doi.org/10.1016/j.chroma.2023.463837.